Surface phonons of C(100)(2X1)-H

AUTHOR(S):

Thachepan, S; Okuyama, H; Aruga, T; Nishijima, M; Ando, T; Mazur, A; Pollmann, J

CITATION:

Thachepan, S ...[et al]. Surface phonons of C(100)(2X1)-H. PHYSICAL REVIEW B 2003, 68(4): 041401.

ISSUE DATE:

2003-07-15

URL:

http://hdl.handle.net/2433/49838

PHYSICAL REVIEW B **68**, 041401(R) (2003)

Surface phonons of C(001)(2×1)-H

S. Thachepan, H. Okuyama, T. Aruga, and M. Nishijima
Department of Chemistry, Graduate School of Science, Kyoto University, Kyoto 606-8502, Japan

T. Ando
National Institute for Material Sciences (NIMS), 1-1 Namiki, Tsukuba, Ibaraki 305-0044, Japan

A. Mazur and J. Pollmann
Institut für Festkörpertheorie, Universität Münster, D-48149 Münster, Germany

(Received 13 March 2003; published 16 July 2003)

Surface phonons of the hydrogen-covered diamond surface C(001)(2×1)-H have been studied by electron energy loss spectroscopy (EELS) combined with semiempirical total-energy calculations. EELS resolves several vibrational features in the energy region of the bulk phonon bands in addition to C-H stretch modes. From calculated depth-resolved spectral densities, the vibrational features are found to originate not only from the adsorbed hydrogen and the carbon surface dimer atoms but also from deeper layers of the diamond crystal. On the other hand, a nearly localized character of the vibrations along the surface is found from the measurements of the energy dispersions.

DOI: 10.1103/PhysRevB.68.041401 PACS number(s): 68.35.Ja, 68.47.Fg, 68.43.Pq

Diamond has attracted much attention from both experimentalists and theorists owing to its intrinsic properties such as a large band gap, high saturation carrier velocity, and high thermal conductivity. Recently, diamond films can be homoepitaxially grown by chemical vapor deposition (CVD) using a mixture of hydrocarbon and hydrogen. It is believed that hydrogen plays a crucial role in the deposition process.[1] Therefore, a study of vibrational properties of hydrogenated diamond surfaces is of great importance since it can lead to a better understanding of the mechanisms governing growth.

A number of experimental,[2–7] as well as theoretical,[8–12] studies has focused on the vibrational properties of C(001)(2×1)-H. The experimental data, mainly obtained using electron energy loss spectroscopy(EELS), show complex vibrational structures ranging from ~120 to 180 meV and a well-defined C-H stretch mode at 362–363 meV.[2–7] Due to their resonance with bulk phonons,[13] the vibrations in the region below 165 meV are not expected to be purely derived from the surface. The assignments of the vibrational losses and their respective displacement patterns, except for the C-H stretch modes, are not clarified yet.

In this study, we investigate vibrational modes of the C(001)(2×1)-H surface by EELS combined with semiempirical total-energy calculations. From the calculations of the depth-resolved phonon spectral densities it is found that the vibrational spectra of C(001)(2×1)-H contain significant contributions from deeper layers of the substrate. The phonon dispersions along the surface are determined from angle-dependent measurements.

The experiments were performed using an ultrahigh vacuum chamber equipped with a high resolution electron spectrometer for EELS (LK-5000, LK Technologies, Inc.), an electron optics for low-energy electron diffraction, and a quadrupole mass spectrometer for gas analysis. The base pressure of the chamber is less than 1×10^{-10} Torr. The B-doped diamond film is epitaxially grown on the (001) surface of synthesized single-crystalline diamond (1*b* type) using microwave plasma-assisted CVD. The thickness of the film is ~20 μm. The typical B concentration in the CVD diamond film is at the ppm level. The size of the sample was $4\times4\times0.3$ mm^3. The sample is mounted on a tantalum holder. The sample can be cooled to 90 K using a liquid nitrogen reservoir, and heated by electron bombardment from the back side. The sample temperature is measured using an alumel-chromel thermocouple attached to the sample holder.

For the EELS measurements, primary energies (E_p) of 1–20 eV, a typical energy resolution of ~3 meV, incidence angles (θ_i) of 60°–80° and emission angles (θ_e) of 25°–80° with respect to the surface normal are used. The phonon dispersion curves are determined along the $\bar{\Gamma}\bar{J}$ and $\bar{\Gamma}\bar{J}'$ high-symmetry lines of the surface Brillouin zone (SBZ) shown in the inset of Fig. 1. Since 2×1 and 1×2 domains coexist on our sample surface, the dispersions along both directions are obtained by the measurements along either direction. We have, therefore, restricted our measurements to the $\bar{\Gamma}\bar{J}'$ line. The length of the respective wave vector parallel to the surface is given by $Q_\parallel = 0.5123\sqrt{E_p}(\sin\theta_i - \sin\theta_e)$ Å^{-1}. All EELS measurements are made at 90 K.

The calculations have been carried out employing the semiempirical total-energy approach (cf. Ref. 10). In the current calculations the convergence with respect to layer number has been improved. The structure optimization has been achieved with 50 C and two H layers (symmetrical slab) while the spectral densities were evaluated for 436-layer slabs (the above 52 plus 384 carbon layers included by bulk filling in the middle of the slab).

Figure 1 and the inset show a series of EELS spectra of C(001)(2×1)-H in the energy region of the bulk phonons (≤165 meV) and the C-H stretch vibrations (~360 meV), respectively, as a function of $Q_\parallel$ at $E_p = 2.8$ eV (the lowest spectrum in Fig. 1), 14.0 eV (the second lowest), and 16.5 eV (the others). In the specular direction ($Q_\parallel = 0$ Å^{-1}), we mainly observe three pronounced losses at 102, 149, and 156 meV. In addition, we find a small peak at 164 meV and a

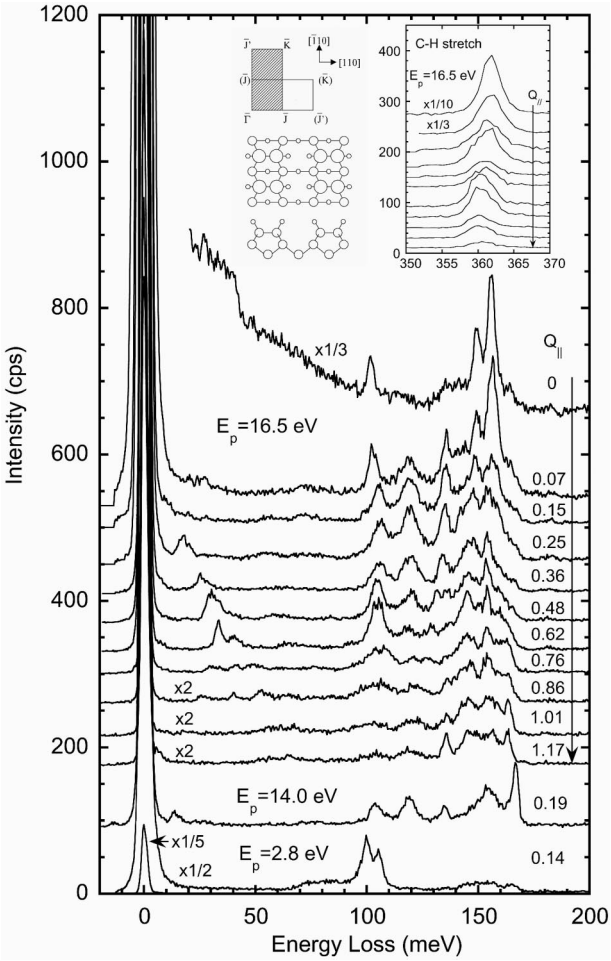

FIG. 1. Series of EELS spectra of C(001)(2×1)-H as a function of $Q_{\parallel}$. The lowest and the second lowest spectra are taken at $E_p=2.8$ and 14.0 eV, respectively, while the others are taken at $E_p=16.5$ eV. The inset shows a top (upper) and a side (lower) view of the C(001)(2×1)-H structural model and the corresponding surface Brillouin zone. The inset shows a series of EELS spectra of the C-H stretch region as a function of $Q_{\parallel}$ at $E_p=16.5$ eV.

broad shoulder at ~135 meV. The asymmetric broad loss centered around ~152–155 meV, observed in previous studies and assigned to the C-H bending mode of the surface dimer,[3,4] is clearly resolved in our spectrum into two peaks at 149 and 156 meV. In the off-specular direction ($Q_{\parallel}=0.07$ Å^{-1}), losses at 120 and 136 meV are clearly detected, in addition, whereas those at 102, 149, and 156 meV are most intense in the specular direction. A small loss is observed at ~70 meV for $Q_{\parallel}=0.07$–0.15 Å^{-1}. We believe that this loss is an intrinsic peak since it is clearly observed at other primary energies (not shown). In the energy region below 65 meV, strongly dispersing features are observed and assigned to the Rayleigh modes in the two directions.[7] At $E_p=14.0$ eV (the second lowest spectrum in Fig. 1), an intense peak is observed at 167 meV. This peak is apparently different from the 164-meV loss observed at $E_p=16.5$ eV. In the $E_p=2.8$ eV spectrum an additional intense loss appears at 100 meV in the off-specular direction.

The loss intensities for C(001)(2×1)-H show a significant dependence on the primary energy E_p (see Fig. 1) indicating that resonance electron scattering occurs.[14] Since the conduction bands of diamond lie above the vacuum level of the C(001)(2×1)-H surface (called negative electron affinity),[15] it is possible that the incoming electrons can temporarily populate conduction bands of the substrate and then be scattered from the surface.

The inset of Fig. 1 shows EELS spectra of the C-H stretch region obtained for $E_p=16.5$ eV and the same $Q_{\parallel}$ values as in Fig. 1. In the specular direction an intense peak is observed at 362 meV. With increasing $Q_{\parallel}$ this peak attenuates and a new peak is observed at 360 meV at $Q_{\parallel}=0.62$ Å^{-1}. One might attribute the 360-meV peak as originating from the dispersion of the 362-meV loss. Instead, we assign these two losses to different normal modes, i.e., to antisymmetric and symmetric stretching modes, for the following reasons: (1) The spectrum at $Q_{\parallel}=0.25$ Å^{-1} consists of two features, a main peak at 362 meV and a shoulder on the low-energy side. Also the main peak at 360 meV for $Q_{\parallel}=0.62$ Å^{-1} has an asymmetric shape with a tailing to higher energies. (2) On Si(001)(2×1)-H, which has a structure similar to C(001)(2×1)-H, the antisymmetric and symmetric stretching modes were clearly resolved by infrared spectroscopy at 259 and 260 meV, respectively.[16,17] (3) Previous calculations for C(001)(2×1)-H showed a negligible dispersion for the two C-H stretching modes (less than 1 meV).[10] Thus we attribute the 360- and 362-meV losses to two different normal modes of the C-H stretch and tentatively assign them, at this point, to the antisymmetric and symmetric modes, respectively. We note that the assignment on the basis of our experimental results is not straightforward because the dipole selection rule[14] may not be applicable on the diamond surface.[4] We come back to this point further below.

In the latest EELS studies of the C(001)(2×1)-H surface, Kinsky *et al.*[7] found a peak at 183 meV which is not observed in Fig. 1. We have used three samples prepared similarly. Only one of them exhibits an unreproducible loss at 183 meV accompanied by a higher-energy tail of the C-H stretch mode. We conjecture that the 183-meV loss is due to minority species on the surface. Indeed, a recent theoretical study predicts that the dihydride species on C(001) shows a CH_2 bending mode at 183 meV.[18] Thus, we attribute the loss at 183 meV reported previously[7] to the dihydride species possibly present at defect sites of the C(001)(2×1)-H surface.

Figure 2 shows calculated atom- and layer-resolved spectral densities at the $\bar{\Gamma}$ point in the energy range of 0–200 meV. They clearly show significant intermixing of the vibrational motions between the surface hydrogen and substrate carbon atoms due to their resonance with the bulk phonons. We find a considerable number of normal modes existing at the $\bar{\Gamma}$ point of the SBZ. Displacement patterns of the most salient of these modes are schematically depicted (not drawn to scale for clarity sake) in Fig. 3. The single-domain 2×1 surface belongs to the C_{2v} point group. Thus, the surface phonon modes can be classified according to the respective irreducible representations, as indicated in Fig. 3. Since we measure spectra of double-domain C(001)(2×1)-H along the $\bar{\Gamma}\bar{J}$ and $\bar{\Gamma}\bar{J}'$ directions at the same time, normal modes of

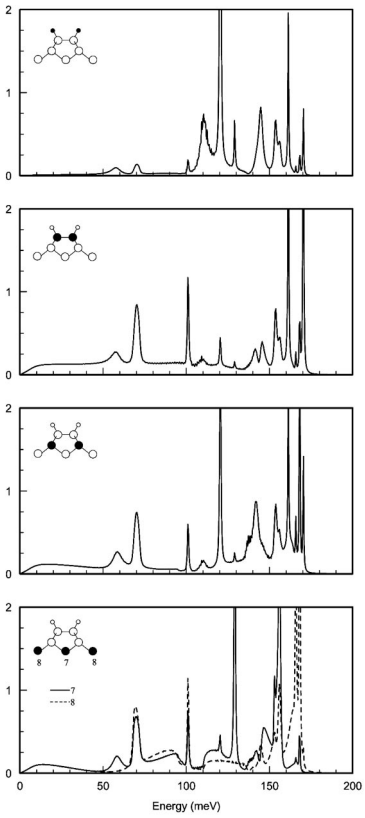

FIG. 2. Calculated atom- and layer-resolved spectral densities in the region of 0–200 meV for the first H adlayer (top panel) and the second, third, and fourth layers of C(001)(2×1)-H. The spectral densities for the two atoms per surface unit cell are identical on the first three layers for symmetry reasons while they are different for atoms 7 and 8.

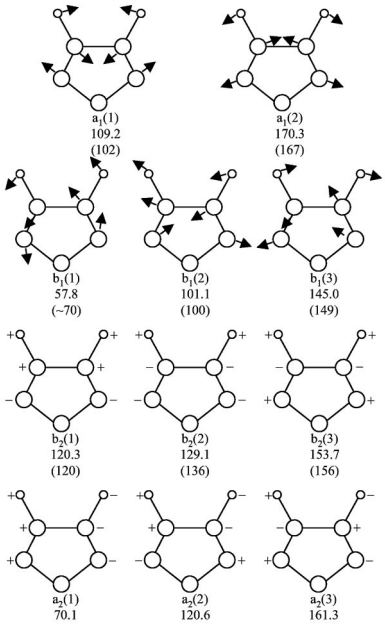

FIG. 3. Schematic displacement patterns of salient normal modes at the Γ point. They are classified according to the irreducible representations of the C_{2v} point group. The calculated energy of each mode, to which an observed loss peak is assigned, is shown with the respective measured energy in brackets (in units of meV). Only the a_1, b_1, and b_2 modes are observable in EELS.

a_1, b_1, and b_2 symmetries can be observed, whereas those of a_2 symmetry are forbidden according to the selection rule for impact scattering[14] and thus cannot be observed by EELS.

The loss peaks are assigned to the calculated normal modes. The ~70 meV loss is assigned to $b_1(1)$. The 100- and 102-meV losses are possibly assigned as $b_1(2)$ and $a_1(1)$, respectively. The 120-, 136-, 149-, and 156 meV losses are assigned to $b_2(1)$, $b_2(2)$, $b_1(3)$, and $b_2(3)$, respectively. As noted above, a previous study assigned the broad loss at ~152–155 meV to C-H bending vibrations.[3,4] We find, however, from the spectral densities that deeper layers of the substrate contribute significantly in this energy region (see Fig. 2). Consequently, the vibrations in this region are attributed to the substrate modes. The 167-meV mode is assigned to $a_1(2)$, which is mainly due to the C-C stretch of the surface dimer. We note at this point that the 120-, 136-, 149-, and 164-meV losses can have significant contributions from the bulk phonons, namely, the transverse optical mode at *W* and *X* and the longitudinal optical mode at *X* and Γ, respectively.[13] Depending on the particular mode, the individual contributions from the first four layers are different, as shown in Fig. 2. For example, the $a_1(2)$ mode, which is mainly due to the C-C stretch of the surface dimer, is localized on the first three layers. The $a_1(1)$ mode is almost completely localized in the H adlayer. It can be called a ''scissors'' mode. On the other hand, a contribution of even the fourth layer is apparent in Fig. 2 for the $b_1(2)$ mode. Figure 3 implies that the $b_2(2)$ mode is characterized by a ''wagging'' motion of the surface dimer. This characterization is not straightforward, however, due to the strong coupling of this mode to the substrate.

To corroborate the general picture of the vibrational modes at the C(001)(2×1)-H surface developed so far, we have investigated, as well, the isotope-substituted C(001)(2×1)-D surface by EELS. For this system we have observed the $a_1(1)$, $b_2(1)$, and $b_1(3)$ modes at 85, 90, and 110 meV, respectively. It is noted that, even if the mode is the same, the displacement patterns for (2×1)-H and (2×1)-D are not exactly the same. These isotope shifts indicate that substantial H (D) motions are involved in these modes which is in agreement with the calculations. We note that the remaining modes for C(001)(2×1)-D are observed nearly at the same energies as those for C(001)(2×1)-H indicating that the effective reduced masses entering these modes are dominated by the C atoms.

Figure 4 shows the wave-vector dependence of the energy losses taken with $E_p = 1$–20 eV, $\theta_i = 60°$–80°, and $\theta_e = 25°$–80°. The calculated phonon bands are shown for comparison by solid curves. For clarity sake, neither the symmetry type nor localization properties of the involved modes are explicitly indicated. Since the dispersion of the losses along both the ΓJ and $\Gamma J'$ directions have to be superimposed under the present experimental conditions, the same experimental results are plotted along both directions. Overall, we find a very good agreement between theory and

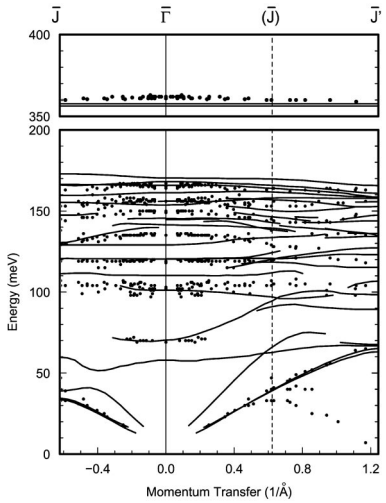

FIG. 4. Surface-phonon dispersions of C(001)(2×1)-H along the ΓJ and $\Gamma J'$ high-symmetry lines. The solid curves represent calculated bands. The modes with small contribution from the surface are not drawn, and thus, some branches are disconnected in the SBZ. The dots show the mode energies, as determined from the EELS data. Since both 1×2 and 2×1 domains coexist at the sample surface, the experimental data are superimposed in both directions. The dashed vertical line indicates the (J) point of the 1×2 SBZ.

experiment for quite a number of bands. To address a few cases the loss observed at 120 meV at $\bar{\Gamma}$ exhibits almost no shift with wave vector, in excellent agreement with the calculated band. The 136-meV loss at $\bar{\Gamma}$ gradually disperses to lower energy splitting into two peaks near $Q_{\parallel}=0.5$ Å^{-1}. The 149-meV loss at $\bar{\Gamma}$ exhibits a shift towards lower energy with increasing $Q_{\parallel}$, where it agrees with calculated bands. The 156-meV loss apparently shifts to 153 meV at $Q_{\parallel}=0.48$ Å^{-1} and shifts back to 156 meV at $Q_{\parallel}=1.17$ Å^{-1}. It is close to respective theoretical bands. The losses near 164 and 167 meV are very close to calculated bands throughout the SBZ. There are some remaining problems. The 136-meV loss may be associated with the upper branch of b_1 character found between ~130 (J) and ~140 ($\bar{\Gamma}$) meV. The 70-meV loss may be associated with the $a_2(1)$ mode due to a slightly relaxed selection rule. The experimental data points associated with the Rayleigh modes are also superimposed from the two domains. The Rayleigh mode along the $\Gamma J'$ direction shows the Umklapp process beyond the (J) point. The measured and calculated energies of the Rayleigh modes at the $\bar{J}$ and $\bar{J'}$ points are 33 and 65 meV, respectively, in accord with previous results.[7] This excellent agreement between our theory and experiment holds for the Rayleigh modes throughout the entire SBZ (see Fig. 4). It should be noted at this point that, for the sake of clarity, the calculated phonon bands are plotted only for the 2×1 SBZ. Thus, they are no superpositions from the 2×1 and the 1×2 SBZ's, as opposed to the experimental data. From Fig. 4 it is obvious, however, that backfolding the calculated bands from $\bar{J}$ to $\bar{\Gamma}$ onto the line from $\bar{\Gamma}\bar{J'}/2$ to $\bar{J'}$ brings the theoretical results into coincidence with the measured Rayleigh modes along both the $J\Gamma$ and $\Gamma J'$ lines. All measured modes, except for the Rayleigh modes, show only small dispersions of less than 5 meV, indicating the localized character of the vibrations along the surface. Some of the calculated bands are not observed in EELS. This is thought to be due to their symmetry or to their weak spectral density. Further up in energy, there occur two C-H stretch modes. One is symmetric with respect to the two C-H bonds (see the side view in the top panel of Fig. 2) while the other is asymmetric. The top panel of Fig. 4 shows the two measured stretch-mode bands around 360 and 362 meV. The calculated stretch-mode bands result to be a little bit lower in energy. We obtain the symmetric stretch mode at 356 and the asymmetric stretch mode at 358 meV from our calculations. The size of the splitting of these two dispersionless bands is practically the same in both experiment and theory, but the symmetry assignment is opposite. The theory yields the symmetric mode to be lower in energy, as compared to the asymmetric mode. This can be rationalized by the fact that the asymmetric stretch mode involves slightly stronger bond-length changes in the H-C-C-H unit, as compared to the symmetric stretch mode.

In summary, we have investigated the vibrational modes for the C(001)(2×1)-H surface by means of EELS combined with semiempirical total-energy calculations. We observe losses at ~70, 100, 102, 120, 136, 149, 156, 164, 167, 360, and 362 meV near the $\bar{\Gamma}$ point. From the calculations of the depth-resolved spectral densities we find that the second or third layers of the diamond substrate significantly contribute to the vibrational spectra of C(001)(2×1)-H. The assignments are made on the basis of our theoretical results. The phonon dispersions along the surface have been determined from angle-dependent measurements, where we find a nearly localized character of the vibrations along the surface.

This work was supported in part by a Grant-in-Aid from the Ministry of Education, Culture, Sports, Science and Technology (Japan).

[1] W.R.L. Lambrecht *et al.*, Nature (London) **364**, 607 (1993).
[2] S.T. Lee and G. Apai, Phys. Rev. B **48**, 2684 (1993).
[3] T. Aizawa *et al.*, Phys. Rev. B **48**, 18 348 (1993).
[4] B.D. Thoms and J.E. Butler, Phys. Rev. B **50**, 17 450 (1994).
[5] B.D. Thoms and J.E. Butler, Surf. Sci. **328**, 291 (1995).
[6] T. Aizawa *et al.*, Diamond Relat. Mater. **4**, 600 (1995).
[7] J. Kinsky *et al.*, Diamond Relat. Mater. **11**, 365 (2002).
[8] D.R. Alfonso *et al.*, Phys. Rev. B **51**, 1989 (1995).
[9] D.R. Alfonso *et al.*, Phys. Rev. B **51**, 14 669 (1995).
[10] B. Sandfort *et al.*, Phys. Rev. B **54**, 8605 (1996).
[11] T. Frauenheim *et al.*, Thin Solid Films **272**, 314 (1996).
[12] K.S. Smirnov and G. Raşeev, Surf. Sci. **459**, 124 (2000).
[13] J.L. Warren *et al.*, Phys. Rev. **158**, 805 (1967).
[14] H. Ibach and D. L. Mills, *Electron Energy Loss Spectroscopy and Surface Vibrations* (Academic, New York, 1982).
[15] J. van der Weide *et al.*, Phys. Rev. B **50**, 5830 (1994).
[16] Y.J. Chabal and K. Raghavachari, Phys. Rev. Lett. **53**, 282 (1984).
[17] J.C. Tully *et al.*, Phys. Rev. B **31**, 1184 (1985).
[18] J.A. Steckel *et al.*, Phys. Rev. B **66**, 155406 (2002).